Atmospheric Transmission at Microwaves (ATM): An Improved Model for Millimeter/Submillimeter Applications

Juan R. Pardo, José Cernicharo, and Eugene Serabyn

Abstract—We present a model of the longwave atmospheric spectrum that improves in many respects widely used older models such as the microwave propagation model (MPM) [1],[2], since it is based on recent broadband measurements and calculations. According to our data, the model is fully applicable from 0 to 2 THz while including lines up to 10 THz. Its primary goal is to simulate the millimeter/submillimeter region accessible from the ground (frequencies up to ~2 THz at most, with a few windows between 1 and 2 THz accessible only under exceptional conditions at very dry sites). Line-by-line calculations of the absorption are performed using a line database generated from the latest available spectroscopic constants for all relevant atmospheric species. The collisional line widths are obtained from published laboratory data. The excess of absorption in the longwave range that cannot be explained by the line spectrum is modeled by introducing two different continuum-like terms based on our own recent FTS measurements between 170 and 1100 GHz: collision-induced absorption of the dry atmosphere due to transient dipoles in symmetric molecules (N_2 and O_2) and continuum-like water vapor opacity. All H_2O lines up to 10 THz are included in order to correctly account for the entire H_2O far-wing opacity below 2 THz for a given line-shape. Hence, this contribution does not need to be part of a pseudocontinuum term below that frequency cutoff (still necessary, as shown in this paper) in contrast to other models used to date. Phase delays near H_2O and O_2 resonances are also important for ground-based astronomy since they affect interferometric phase. The frequency-dependent dispersive phase delay function is formally related to the absorption line shape via the Kramers–Krönig dispersion theory, and this relation has been used for modeling those delays. Precise calculations of phase delays are essential for the future Atacama large millimeter array (ALMA) project. A software package called atmospheric transmission at microwaves (ATM) has been developed to provide the radioastronomy and aeronomy communities with an updated tool to compute the atmospheric spectrum in clear-sky conditions for various scientific applications. In this paper, we use this model to provide detailed simulations of atmospheric transmission and phase dispersion for several sites suitable for submillimeter astronomy.

Index Terms—Atmospheric measurements, microwave radio propagation, radio astronomy, software packages, submillimeter-wave spectroscopy.

J. R. Pardo and J. Cernicharo are with the Division of Physics, Mathematics, and Astronomy, California Institute of Technology, Pasadena, CA 91125 USA (e-mail: pardo@submm.caltech.edu) and the Instituto de Estructura de la Materia, Departamento de Física Molecular, CSIC, Madrid, Spain.

E. Serabyn is with the Division of Physics, Mathematics and Astronomy, California Institute of Technology, Pasadena, CA 91125 USA.

I. Introduction

ACCURATE modeling of the longwave emission/absorption spectrum of the terrestrial atmosphere is needed in many scientific applications. In the astrophysical domain, it is needed to predict the atmospheric attenuation at a given frequency for ground based and airborne observatories in order to calculate system noise temperatures as well as to estimate phase delays for interferometry. In remote sensing of the atmosphere and the Earth's surface, obtaining useful data for meteorological and environmental studies relies upon an accurate knowledge of the atmospheric spectrum.

In the longwave domain, several models have been widely used to date. The astrophysical community has mainly used the following models: atmospheric transmission (AT) [3]; atmospheric transmission at microwaves (ATM) [4]–[6]; several codes developed on the basis of Liebe's microwave propagation model (MPM), [1], [2], which is also extensively used by the aeronomy and remote-sensing communities; and radiative transfer codes based on different well-known line databases— HITRAN [7], JPL [8], and GEISA [9].

Most of the above models do not provide a high degree of accuracy or are incomplete for two principal reasons: lack of correct description of the continuum-like opacity between resonant features and lack of consideration of phase dispersion. The model we present here is the result of several years of work on both the modeling and the experimental sides and is aimed at computing opacity, radiance, phase delay, and polarization along a given path in the terrestrial atmosphere at millimeter and submillimeter wavelengths. Polarization can be produced by different mechanisms: emission of paramagnetic molecules such as O_2 under the effect of the geomagnetic field, radiation scattering by hydrometeors, or reflection on a Fresnel-like (ocean) surface. These mechanisms are also treated in the ATM model but have been ([10]–[12] Zeeman effect) or will be discussed elsewhere ([13] scattering by hydrometeors). Here we discuss only unpolarized radiative transfer through a clear sky.

In Section II, we give an overview of the unpolarized radiative transfer theory with some definitions that will be used throughout this paper. The basic theoretical aspects regarding calculations of the resonant absorption of the atmosphere are given in Section III. Different spectroscopic parameters are reviewed in Section IV. A discussion comparing our formulation to the widely used MPM models [1], [2] is given in Section V to show how our treatment improves those works (Liebe's empirical models are otherwise difficult to link to the quantum mechanical properties of the molecules considered in the models).

Line shapes are discussed in Section VI. The continuum likeabsorption is treated in Section VII. We present some results of our Fourier transform spectroscopy (FTS) measurements on Mauna Kea in Section VIII to illustrate the accuracy of the model. Section IX then focuses on the astrophysical utility of the code. In particular, it is used to predict atmospheric attenuation, atmospheric emissivity, and phase delay over a wide range of frequencies for several potential and present submillimeter observatory sites. Finally, Section X provides a summary.

II. UNPOLARIZED RADIATIVE TRANSFER

The unpolarized radiative transfer in nonscattering media is described by a relatively simple differential scalar equation [14]

$$\frac{dI_\nu(\vec{r}, \vec{n})}{ds} = \epsilon_\nu - \kappa_\nu I_\nu(\vec{r}, \vec{n}) \qquad (1)$$

where

I_ν	radiance (in Wm^{-2} $ster^{-1}$ cm^{-1});
$\epsilon_\nu dw d\nu ds d\sigma$ and $\kappa_\nu I(\vec{r}, \vec{n}, \nu) dw d\nu d\sigma ds$	amounts of energy emitted and absorbed at frequency ν in a pencil of solid angle dw in the direction $\vec{r}$ through a cylinder of length ds and cross section $\vec{d\sigma} = d\sigma \vec{n}$;
ϵ_ν and κ_ν	macroscopic absorption and emission coefficients.

The absorption coefficient gives the fractional loss of intensity (at a given wavelength) per length through an absorbing medium.

After rearranging (1), the radiative transfer problem is unidimensional in the direction of $\vec{r}$ in the absence of scattering. We can formulate the problem under local thermal equilibrium (LTE) conditions as follows:

$$\frac{dI_\nu(s')}{d\tau_\nu} = -I_\nu(s') + S_\nu(T[s']) \qquad (2)$$

where

s'	coordinate along the path;
$S_\nu = \epsilon_\nu / \kappa_\nu$	source function;
$d\tau_\nu = \kappa_\nu ds$	differential opacity.

The solution of this equation can be given in an integral form

$$I_\nu(s) = I_\nu(0) e^{-\tau_\nu(0,s)} + \int_0^s S_\nu(s') e^{-\tau_\nu(s',s)} \kappa_\nu(s') ds'. \qquad (3)$$

For ground-based measurements, $I_\nu(0)$ is commonly taken as the radiance from the *cosmic background.*

However, to actually solve the last equation, a complete knowledge of κ_ν as a function of position—which implies a knowledge of the abundance properties of all contributing molecules—and of the lineshape is needed. To perform radiative transfer calculations through the atmosphere in particular situations, some well-known physical approximations can be assumed. For example, the physical medium under study contains only $\sim 0.001\%$ of its mass above an altitude of 90 km,

where in addition, most molecules are strongly dissociated due to solar ultraviolet radiation, thus limiting the vertical range needed for the calculations. Only for O_2, Zeeman splitting calculations do higher altitudes need to be considered [10], [11]. Furthermore, within the 0–90 km vertical range, typical temperatures are ~ 220 to 320 K and typical pressures range from ~ 1020 to 0.0015 mb. Under these physical conditions, the populations of the different energy levels of a given species in a small volume of atmospheric gas are fully controlled by collisions, and thus depend only on the local physical temperature T (the local thermodynamic equilibrium, or LTE, approximation). Collisional rates fall with altitude, and pumping by solar photons will start to dominate the population of the molecular levels at some point above the high mesosphere (> 80 km), making the LTE approximation fail. At these altitudes, however, the contribution from the different molecular species to the atmospheric opacity in the millimeter, submillimeter, and far-infrared wavelength domains is negligible.

To compute the output radiance arising from a propagation path in the atmosphere, we need to know the functions $T(s)$ (physical temperature along the path, which determines the local source function and also enters into the absorption coefficient [see (9)], $P(s)$, and the number densities of the different atmospheric gases $N_i(s)$. We divide the total path into a number of steps and then discretize the integral for numerical calculations to achieve an accuracy on the order of 0.1 K. The geometry for calculations can be plane-parallel for zenith (or nadir) angles up to $\sim 75°$. A spherical geometry must be considered for higher zenith (or nadir) angles and for limb paths, which our model can also provide. At the end, the code converts the output radiance I_ν into an equivalent blackbody temperature $T_{EBB,\nu}$ simply by inverting the Planck function.

III. LINE ABSORPTION: GENERALITIES

Unless otherwise indicated, the units used in this paper and internally in the code are the following:

1) Frequency: GHz;
2) pressure: mb;
3) temperature: K;
4) absorption: m^{-1};
5) number density: m^{-3};
6) phase delay: $deg \cdot m^{-1}$;
7) spectroscopic constants: MHz;
8) electric or magnetic dipole moments: Debyes (1 Debye = 10^{-19} esu $\cdot$ cm).

In general, the line-by-line integrated opacity corresponding to a path through the terrestrial atmosphere is calculated as follows:

$$\tau_\nu = \sum_{i(\text{layers})} \left[\sum_{j(\text{molec.})} \left(\sum_{k(\text{lines})} \kappa_{\nu_k} \right)_j \right]_i \cdot \Delta s_i \qquad (4)$$

where Δs_i is the path through the homogeneous ith layer and no line coupling between different species is assumed. As pressure increases, the program uses thiner layers to follow the opacity distribution.

Let us consider the process of line absorption between two energy levels l and u. In principle, it takes place only at the frequency $\nu_{l \to u}$, and each photon absorbed or emitted corresponds to a loss or gain of one quantum of energy $h\nu_{l \to u}$. So

$$dI_{\nu_{l \to u}} = -\left(\frac{N_l}{g_l} - \frac{N_u}{g_u} \right) R_{l \to u} h\nu_{l \to u} ds \quad (5)$$

where

$R_{l \to u}$ transition rate for $l \to u$;
$N_{l,u}$ populations of the energy levels;
$g_{l,u}$ their degeneracies.

From the microphysical point of view, this rate equals to $B_{l \to u} I_{\nu_{l \to u}}/c$, where $B_{l \to u}$ is the Einstein transition coefficient for stimulated absorption, given by [15]

$$B_{l \to u} = \frac{2\pi}{3\hbar^2} |< u \mid \mu \mid l >|^2 \quad (6)$$

where μ is the dipole operator of the transition and $\mid u >$, $\mid l >$ are the wavefunctions of the upper and lower states. Finally, we have to take into account that several line-broadening mechanisms spread the absorptions around the theoretical resonant frequency $\nu_{l \to u}$. This is taken into account by introducing a line shape function $f(\nu, \nu_{l \to u})$. The absorption coefficient of a rotational transition of a polar molecule thus becomes

$$(\kappa_\nu)_{lu} = \frac{8\pi^3 \nu}{3hc} \left[\frac{N_l}{g_l} - \frac{N_u}{g_u} \right] |< u \mid \mu \mid l >|^2 f(\nu, \nu_{l \to u}). \quad (7)$$

The last equation is general. We will now discuss its various parts in order to arrive at the formulation actually used in our code.

The collisional relaxation rate under the considered atmospheric conditions is fast enough to maintain a Boltzmann distribution of the energy-level populations (see Section II). The Boltzmann equation under equilibrium conditions indicates $N_u/g_u = (N_l/g_l)\exp[-(E_u - E_l)/kT]$ and the fractional population of molecules in the nth state is given by

$$\frac{N_n}{N} = g_n \frac{\exp\left(\frac{-E_n}{kT} \right)}{Q} \quad (8)$$

with E_n being the energy level of the state and g_n its degeneracy. Q is the partition function $[Q = \sum_i g_i \exp(-E_i/kT)]$. In the case of the Born–Oppenheimer approximation (which holds for the relatively simple molecules to be considered in the atmosphere), the wavefunction is the product of electronic, vibrational, rotational, and nuclear spin functions. So, we can apply to the population of a given molecular species the product of vibrational and rotational partition functions. Introducing (8) into (7), we have

$$(\kappa_\nu)_{lu} = \frac{8\pi^3 N\nu}{3hcQ} \left(e^{-E_l/kT} - e^{-E_u/kT} \right) \cdot |< u \mid \mu \mid l >|^2 f(\nu, \nu_{l \to u}) \quad (9)$$

where N is the number density in the relevant vibrational state of the molecule in question. This is the basic expression used in our model.

IV. SPECTROSCOPIC PARAMETERS

We discuss in this section the calculation of the different parts of (9) that we have performed to create the database used in the model. Only a few parameters have been taken from other existing databases (see below).

The intensity of the transitions is determined by the transition probabilities and by the population factors. Both transition probabilities and rotational energy levels (from which both line frequencies and population factors under LTE can be determined) can be obtained from the rotational Hamiltonians. This allows us to build a compact database since spectroscopic line parameters can be derived from a small number of parameters, the rotational constants of the molecular species.

The number of rotational constants to be considered varies for linear molecules, symmetric top molecules, and general asymmetric rotors (the types of molecules we find in the atmosphere). The expressions for those Hamiltonians that we have considered are as follows.

1) *Diatomic or linear molecules (with no magnetic moment):* The rigid rotor Hamiltonian $H = BJ^2$ is usually corrected to introduce the centrifugal distortion correction, giving the energy levels and transition frequencies as follows:

$$E = BJ(J+1) - DJ^2(J+1)^2 + HJ^3(J+1)^3 \quad (10)$$

$$\nu = 2B(J+1) - 4D(J+1)^3 + H(J+1)^3[(J+2)^2 - J^3] + \cdots \quad (11)$$

where J is the rotational quantum number and B, D, and H are rotational constants.

2) *Symmetric rotor in $^3\Sigma$ electronic state*

$$H = B \cdot N^2 + \alpha N \cdot S + \frac{2}{3}\beta(3S_z^2 - S^2) \quad (12)$$

where S is the electronic spin operator, N is the orbital + rotational angular moment, and B, α, and β are rotational constants.

3) *Asymmetric rotors:* We use the Watson-type Hamiltonian [16] according to the notation appearing in [17].

A. Transition Probability

We parametrize the transition probability as follows:

$$|< J, \tau \mid \mu \mid J', \tau' >|^2 = \mu_g^2 \lambda_g(J, \tau, J', \tau').$$

J, J' represent rotational quantum numbers, τ, τ' are other quantum numbers, μ_g is the value of the dipole moment (electric or magnetic), and $\lambda_g(J, \tau, J', \tau')$ is a dimensionless parameter called oscillator strength of the particular transition.

B. Partition Function

The case of symmetric linear or diatomic molecules ($^{16}O_2$, N_2O [linear] or CO), and the general asymmetric rotors must be treated individually. In the first case, the energy levels are $\sim hBJ(J+1)$, where B is the rotational constant of the molecule in the considered vibrational state. There are corrections to this simple rigid rotor expression already explained [see (10) and

(11)] but for CO, the parameter D is five orders of magnitude smaller than B. For other important atmospheric molecules, the ratio B/D is even larger. So, if the molecule is heteronuclear and has no nuclear spin; the degeneracy of the rotational levels (represented by the quantum number J) is $2J + 1$ and we can write

$$Q_r \simeq \sum_J (2J + 1) \exp\left[\frac{-hBJ(J+1)}{kT}\right]. \quad (13)$$

For the considered atmospheric temperature range, it is convenient to use the expansion series of Herzberg [18]

$$Q_r = \frac{kT}{hB} + \frac{1}{3} + \frac{1}{15}\frac{hB}{kT} + \frac{4}{315}\left(\frac{hB}{kT}\right)^2 + \cdots. \quad (14)$$

The number of terms to be considered in this expansion depends on the ratio of kT/hB. For example, for CO and a temperature of 250 K, $kT/hB = 90.42$, and this value is even larger for N_2O and other linear or diatomic molecules in the atmosphere. The approximation of taking the first term of this series is good within $\sim 0.4\%$ and has been adopted in our code. However, the real partition function for $^{16}O_2$ is not kT/hB (as it is for $^{16}O^{18}O$) because this molecule has a center of symmetry. The factor $2J + 1$ in (13) has to be replaced by $\eta(J)[2J + 1]$, with $\eta(J)$ being zero if J is even and 1 if J is odd. In that case, the approximation for the partition function is $Q_r = 3kT/2hB$, the factor three coming from the spin degeneracy.

In the case of asymmetric rotors (O_3, SO_2, ...), there are three main rotational constants (A, B, C) in the Hamiltonian related with the three principal axes. There are also corrections due to centrifugal and other effects. Herzberg [18] also found an approximation for the partition function in this case, the validity of which is equivalent to the one we have seen for linear or diatomic molecules. It is

$$Q_r = \left(\frac{\pi k^{\frac{3}{2}}}{\sigma}\right)\left(\frac{T^3}{ABC}\right)^{\frac{1}{2}} = \left(\frac{5.34 \cdot 10^6}{\sigma}\right)\left(\frac{T^3}{ABC}\right)^{\frac{1}{2}} \quad (15)$$

where σ is the order of the symmetry group to which the molecule belongs in the considered electronic and vibrational state (for example, O_3 in the ground electronic and vibrational state is a C_{2v} molecule $\Rightarrow \sigma = 2$).

C. Rotational Constants

In Table I, we give the bibliographical sources for the rotational constants of the different molecular species needed to reproduce the atmospheric spectrum as seen from the ground. Those molecules are listed in our previous works [19], [20]. Other molecules have to be considered for limb sounding simulations, and some of them are also listed in the same table. Of these molecules, $^{16}O_2$ and $H_2^{16}O$ need special attention because they determine the general shape of the tropospheric spectrum in the frequency range considered here (especially $H_2^{16}O$).

The dipole moments and Hamiltonians we have used to determine the line parameters for the oxygen and water species come from the references in Table I. Line-broadening parameters mostly come from the HITRAN database. A recent work

TABLE I
ALL MOLECULES INCLUDED IN THE ATM MODEL. THOSE MARKED WITH AN ASTERISK APPEAR IN OUR 200-MHz-RESOLUTION FOURIER TRANSFORM SPECTROSCOPY DATA AFTER A BRIEF INTEGRATION TIME [19], [20]

Molecular species	Reference
(*) $H_2^{16}O$	Matsushima et al [22]
(*) $H_2^{18}O$	Helminger and De Lucia [23]
$H_2^{17}O$	"
(*) $H_2^{16}O$ (0,1,0)	Belov et al [24]
(*) HDO	De Lucia et al [25]
(*) $^{16}O_2$	Zink & Mizushima [26]
$^{16}O_2$ v=1	"
(*) $^{16}O^{18}O$	Steinbach & Gordy [27]
$^{16}O^{17}O$	Gordy & Cook [28]
(*) $^{16}O_3$	Pickett et al [29]
$^{16}O_3$ (0,1,0)	"
$^{16}O_3$ (1,0,0)	Flaud et al [30]
$^{16}O_3$ (0,0,1)	"
$^{16}O^{16}O^{18}O$	Flaud et al [31]
$^{16}O^{18}O^{16}O$	"
$^{16}O^{16}O^{17}O$	Rinsland et al [32]
$^{16}O^{17}O^{16}O$	"
N_2O	Andreev et al [33]
CO	Gordy & Cook [28]
SO_2	Helminger & de Lucia [34]
SH_2	Lane et al [35]
NO_2	Semmoud-Monnanteuil et al [36]

([21]) providing laboratory measurements of 17 new $H_2^{16}O$ (0,0,0) and (0,1,0) lines between 0.8 and 1.6 THz gives an update on the available water line frequencies. This list has been compared with our calculations with satisfactory results within current experimental accuracy.

V. COMPARISON TO MPM

The MPM models [1], [2] have been widely used by the remote-sensing community during the past. Especially for submillimeter applications, those models present several problems.

1) The dry continuum term is off by $\sim 29\%$ according to our measurements presented in [20].
2) No lines above 1 THz are included.
3) H_2O excess pseudocontinuum absorption in the submillimeter range is introduced in different ways through the different versions of the model. None of those descriptions is in good agreement with submillimeter data [20].
4) Ozone and other minor components not included.
5) The parametrizations of the line absorption of water vapor and molecular oxygen is very hard to link to "fundamental" parameters such as oscillator strengths and energy levels. In addition, some line parameters have problems. This is described in detail in the remainder of this section.

Liebe's MPM models give the H_2O and O_2 resonant part of the atmospheric spectrum as follows:

$$\kappa_\nu = C \cdot \nu \sum_k S_k F_k(\nu), \quad C = 4.1907 \cdot 10^{-5} \quad (16)$$

using as input parameters the partial pressure of H_2O (p_w), that of the dry air (p_d) and the parameter $\theta = 300/T$, where T is the physical temperature.

S_k (which is a "line strength") is parametrized as follows:

$$O_2: \quad S_k = \frac{a_{1k}}{\nu_k} p_d \theta^3 \exp[a_{2k}(1 - \theta)]$$

$$H_2O: \quad S_k = \frac{b_{1k}}{\nu_k} p_w \theta^{3.5} \exp[b_{2k}(1 - \theta)].$$

The parameters ν_k (line frequencies in gigahertz), a_{1k}, b_{1k} (Hz/Pa), and a_{2k}, b_{2k} (both dimensionless) are tabulated through a series of papers. The difference in the exponent of θ (3.5 for H_2O and 3 for O_2) comes simply from the fact that water vapor is an asymmetric top molecule and O_2 is symmetric so that the partition function of water is $\propto T^{3/2}$, while for oxygen is $\propto T$ (16). $F_k(\nu)$ is in general a complex line shape function like $\mathcal{F}$ (27) or (28) but normalized in a different way. Its imaginary part relates with our line-shape function $f(\nu, \nu_{l \to u})$ (20) and (21) as follows: $F_k(\nu, \nu_{l \to u}) = \pi \nu_{l \to u} f(\nu, \nu_{l \to u})$.

Since Liebe makes his calculations in terms of refractivity, it is only the imaginary part of his function that needs to be compared to our absorption formulation (9). For this comparison, it is beneficial to make the following approximation (valid only at low frequencies)

$$e^{-E_0/KT} - e^{-E_1/KT} = e^{-E_0/KT}[1 - e^{-h\nu_k/KT}]$$
$$\simeq (h\nu_k/kT)e^{-E_0/KT}$$

since it appears to be the basis of Liebe's parameterization. Eliminating elements that are repeated in both cases, we have (note that $\nu_{l \to u} \equiv \nu_k$)

$$O_2: \quad C \cdot a_{1k} p_d \theta^3 e^{a_{2k}(1-\theta)} = \frac{8\pi^2 N_{o_2} v_k}{3cQkT}$$
$$\times e^{-\frac{E_0}{kT}} S_k \mu_B^2$$

$$H_2O: \quad C \cdot b_{1k} p_w \theta^{3.5} e^{b_{2k}(1-\theta)} = \frac{8\pi^2 N_{H_2o} v_k g_k}{3cQkT}$$
$$\times e^{-\frac{E_0}{KT}} g_k S_k \mu^2. \quad (17)$$

Other elements in (17) that we can explicitly give are

$\dfrac{O_2}{p_{o2}=0.2097p_d=N_{o_2}kT}$	$\dfrac{H_2O}{p_w=N_{H_2o}kT}$
$Q = \dfrac{3kT}{2hB}$	$Q = \left(\dfrac{5.34 \cdot 10^6}{\sigma[-2]}\right)\left(\dfrac{T^3}{ABC}\right)^{\frac{1}{2}}$
	$A = 835\,839.876 \text{ MHz}$
$B = 43\,100.430 \text{ MHz}$	$B = 435\,346.811 \text{ MHz}$
	$C = 278\,140.481 \text{ MHz}$
$\mu_B = 1.854 \cdot 10^{-2} \text{ Debyes}$	$\mu = 1.88 \text{ Debyes}$

Introducing all of the above into (17), we finally arrive at

$$O_2: \quad \nu_k(GHz)S_k e^{\frac{-E_0}{kT}} = 24.717 a_{1k}\left(\frac{\text{Hz}}{\text{Pa}}\right)$$
$$\times \exp(a_{2k})e^{\frac{-a_{2k}}{kT}} \quad (18)$$

$$H_2O: \quad b_{1k}\left(\frac{Hz}{Pa}\right)e^{b_{2k}}e^{\frac{-b_{2k}}{kT}} = 2358.852\nu_k(GHz)$$
$$\times S_k g_k e^{\frac{-E_0}{kT}}. \quad (19)$$

It follows that:
1) a_{2k} (no units) $= E_0(K)/300$;
2) $\nu_k(\text{GHz})S_k/a_{1k}(\text{Hz/Pa})exp(a_{2k}) = 24.717$;
3) b_{2k} (no units) $= E_{0k}(K)/300$;
4) $b_{1k}(\text{Hz/Pa})exp(b_{2k})/\nu_k(\text{GHz})\mathcal{S}_k g_k = 2358.852$.

For the spin-rotation O_2 lines around 60 GHz, 2) above is valid within 0.2%. For the H_2O resonance at $\nu_k = 325.1529$ GHz, $g_k = 1$ and $\lambda_k = 0.091$. Liebe gives for the same resonance $b_{1k} = 14\,990$ and $b_{2k} = 1.540$, so that item 4) is also true within 0.2%. However, all four identities rely upon the validity of the approximation $1 - e^{-h\nu_k/kT} \simeq h\nu/kT$, so that the parameters a_{1k}, a_{2k}, b_{1k}, and b_{2k} are artificially adjusted beyond the Rayleigh–Jeans regime. Such an artifice is not necessary in our case. In addition, for the 22.24- and 183.31-GHz resonances, Liebe gives experimental values that make ratio, (see item 4), fail by 7%.

VI. LINE SHAPES

A. Absorption

In this section, we deal only with the function $f(\nu, \nu_{l \to u})$ as it appears in (9).

In the microwave domain, the natural line width (related to the spontaneous emission lifetime) is on the order of 10^{-6} Hz and is completely negligible when compared with other broadening mechanisms taking place in the atmosphere.

In the lower atmospheric layers (up to ~50 km, depending on the molecule and the criteria), the collisional broadening mechanism (also called pressure broadening) dominates the line shape. The proximity of other molecules introduces perturbations in the Hamiltonian of the molecule under study. Thus, the position of its energy levels change and so the frequencies of different transitions are affected. The most general description of the collisional shape of lines and bands of overlapping lines has been given by Fano [37]. One approximation considers that the time between collisions τ_{col} ($\propto P^{-1}$) is much shorter than the time for spontaneous emission τ_{rad}, which is, in the case of a two-level system, $1/A_{u \to l}$, where $A_{u \to l}$ is the Einstein's coefficient for spontaneous emission. This approximation leads to the Van Vleck–Weisskopf (VVW) profile [38], normalized as follows to be included in (9):

$$f_{\text{VVW}}(\nu, \nu_{l \to u}) = \frac{\nu \Delta\nu}{\pi \nu_{l \to u}}\left(\frac{1}{(\Delta\nu)^2 + (\nu - \nu_{l \to u})^2}\right.$$
$$\left. + \frac{1}{(\Delta\nu)^2 + (\nu + \nu_{l \to u})^2}\right). \quad (20)$$

A different approximation, leading to the kinetic line shape (Zhevakin and Naumov [39]), considers the case in which τ_{col} is much longer than τ_{rad}. The line profile is then

$$f_{\text{ZN}}(\nu, \nu_{l \to u}) = \frac{2\nu_{l \to u}\nu\Delta\nu}{\pi(\nu_{l \to u}^2 - \nu^2)^2 + 4\nu^2\Delta\nu^2}. \qquad (21)$$

For most trace atmospheric molecules, the pressure-broadening parameter $\Delta\nu$ is on the order of 2–3 MHz/mb [44]. In the impact approximation, the collisional broadening parameter is on the order of $1/2\pi\tau_c$. This approximation proves to work quite well within a given distance from the line centers. For example, all the millimeter/submillimeter lines of H_2O and other molecules up to 1.2 THz are well reproduced using this approximation within that frequency range [19],[20]. However, H_2O resonances located at higher frequencies introduce some far-wing absorption below 1.2 THz that is not equal to what is predicted from those lines simply using a VVW profile. This may be due to the finite collision time. Due to the complexity of the calculations and the lack of precise laboratory data, it has been simpler to add a pseudocontinuum opacity at millimeter and submillimeter wavelengths to account for this excess absorption (see Section VII). The broadening parameter also depends on the velocities of particles, i.e., it depends on temperature. This dependence ultimately will be controlled by the type of intermolecular potential. A classic type of interaction in the atmosphere is the one between an asymmetric top molecule (C_{2v} group; for example, H_2O or O_3) and a symmetric molecule (O_2 and N_2). The potential can be written as a sum of the molecular electrostatic contributions and atom–atom contributions [40]. For laboratory measurements of the collisional broadening parameter and its temperature dependence, the following expression is usually adopted [41]

$$\Delta\nu(P,T) = \Delta\nu(P_0,T_0)\frac{P}{P_0}\left(\frac{T_0}{T}\right)^\gamma. \qquad (22)$$

Laboratory measurements provide $\Delta\nu(P_0,T_0)$ and γ, and the results are tabulated in the spectroscopic databases.

In the atmosphere, we neglect the effect of self-collisions of trace gases (for example, for O_3, we neglect $O_3 - O_3$) and we consider collisions of only two types: self-collisions of abundant molecules (O_2 and H_2O) and collisions involving all species with one of the two main atmospheric components (O_2 and N_2). From the works of Connor *et al.* [42], Gamache *et al.* [43], Bouazza *et al.* [44], and others, the following "addition" law for the collisional broadening parameters of molecule M is suggested:

$$\Delta\nu(M - \text{dry air}) = X_{N_2}\Delta\nu(M - N_2) + X_{O_2}\Delta\nu(M - O_2) \qquad (23)$$

where X are the volume mixing ratios. The P and T dependence is implicit. Laboratory measurements for individual lines are the only source of precise information about the parameters γ and $\Delta\nu(M - N_2)$ for the different atmospheric trace gases. The exponent γ has been found in most cases to be in the range 0.6 to 1.0. Thus, taking into account the range of atmospheric

temperatures and pressures that we are considering, it is clear that the well-known linear pressure dependence plays a much more important role than the temperature exponent γ on the collisional width. This is the reason that limb sounding systems use the linewidths to establish the pressure (vertical) grid [45].

The only atmospheric molecule other than O_2 for which self-collisions have to be considered is H_2O. Such self-collisions play an important role on the shape of the strong atmospheric lines of this molecule in the lower troposphere. For self-collisions, the temperature exponent is 1.0. However, for the high-altitude sites considered below, this term is negligible.

When the pressure gets very low, the Doppler effect due to the random thermal molecular motion dominates the line broadening. If we calculate the distribution of frequencies close to a molecular resonance from a sample of molecules whose velocities are described by a Maxwellian distribution, one obtains a Gaussian line shape, which we normalize as follows to be compatible with (7)

$$f_D(\nu, \nu_{l \to u}) = \frac{1}{\Delta\nu_D}\left(\frac{\ln 2}{\pi}\right)^{\frac{1}{2}} exp\left[-\left(\frac{\nu - \nu_{l \to u}}{\Delta\nu_D}\right)^2 \ln 2\right] \qquad (24)$$

where the half-width parameter is given by

$$\Delta\nu_D = \frac{\nu_{l \to u}}{c}\sqrt{\frac{2\ln 2kT}{m}} = 3.58 \cdot 10^{-7}\nu_{l \to u}\sqrt{\frac{T}{M}} \qquad (25)$$

where M is the molecular weight of the species in g/mol.

If the collisional and thermal broadening mechanisms are comparable, the resulting line-shape is the convolution of a Lorentzian (collisional line shape at low pressures) with a Gaussian, generally called Voigt profile

$$f_V(\nu, \nu_{l \to u}) = \int_{-\infty}^{\infty} f_L(\nu, \nu')f_D(\nu', \nu_{l \to u})d\nu'. \qquad (26)$$

B. Phase Delay

Besides absorption, molecular lines introduce a phase delay to the propagation of waves through the atmosphere. It is called the dispersive phase delay (there is also a nondispersive one that is simply related to the fact that the atmosphere has a refractive index different of 1 independently of the presence of molecular lines). This dispersive phase delay increases as the wavelength approaches that of a molecular line, with a sign change across the line center. The process can be understood as a forward scattering by the molecular medium in which the phase of the radiation changes. In the following we will refer only to the dispersive phase delay and we will call it simply "phase delay."

Both the absorption coefficient and the phase delay can be treated in a unified way for any system since both parameters are derived from a more fundamental property, the complex dielectric constant, by means of the Kramers–Krönig [46],[47] relations. Application of the Kramers–Krönig theory to evaluate phase dispersion allows our model to make predictions for future submillimeter interferometry sites.

A generalized (complex) expression of the VVW profile, which accounts for both the Kramers–Krönig [46], [47] disper-

sion theory and line overlapping effects (parameter δ; [48]) is the following ($\nu_{l \to u} \equiv \nu_{lu}$):

$$\mathcal{F}_{\text{VVW}}(\nu, \nu_{lu}) = \frac{\nu}{\pi \nu_{lu}} \left[\frac{1 - i\delta}{\nu_{lu} - \nu - i\Delta\nu} + \frac{1 + i\delta}{\nu_{lu} + \nu + i\Delta\nu} \right] \tag{27}$$

the imaginary part of which reduces to (20) for f_L when $\delta = 0$.

The complex expression of the kinetic line profile [49] is

$$\mathcal{F}_G(\nu, \nu_{l \to u}) = \frac{2\nu_{l \to u} \cdot (\nu_{l \to u}^2 - \nu^2 + i\nu\Delta\nu)}{\pi(\nu_{l \to u}^2 - \nu^2)^2 + 4\nu^2\Delta\nu^2}. \tag{28}$$

VII. Continuum-Like Absorption

The earliest attempt to introduce an empirical continuum correction at millimeter wavelengths was made by Gaut and Reifenstein [50]. Measurements of this absorption in the millimeter domain were first performed by Rice *et al.* [51]. Recently, Serabyn *et al.* [19] and Pardo *et al.* [20] have accurately measured the continuum-like terms across the submillimeter range.

A. Review of the H_2O Pseudocontinuum

Since we include lines with frequencies only up to 10 THz and the true far-wing lineshape is not known accurately, a broadband "continuum"-like absorption term needs to be included (e.g., [52] and [53]). If the far wings are not well reproduced by an assumed collisional line shape or too few lines are included in the summation, a residual (negative or positive) opacity remains. For example, as explained in Section VI-A, failure of the impact-approximation line shape is expected below 1.2 THz for the far wings of those H_2O lines centered above 1.2 THz. Ma and Tipping [54] performed a rigorous study of the water vapor "self-broadened" pseudocontinuum term (involving binary collisions of water molecules) at millimeter and submillimeter wavelengths, but not of foreign gas broadening, likely the dominant effect at high altitudes. Clough *et al.* [52] define a "foreign" pseudocontinuum absorption (for collisions of H_2O with either O_2 or N_2) by considering far wings ($\mid \nu - \nu_i \mid \geq 25 \, \text{cm}^{-1}$) of all water vapor lines from 0 to 10 000 cm^{-1} and making a semiempirical correction to the line shape of the impact approximation.

B. Dry Continuum-Like Absorption

The continuum-like absorption of the dry atmosphere is made up of two components. 1) Collision-induced absorption due to transient electric dipole moments generated during binary interactions of symmetric molecules with electric quadrupole moments such as N_2 and O_2 and 2) the relaxation (Debye) absorption of O_2. The physical explanation of the second term is the following: in the presence of incident radiation of frequency ν, the oxygen molecule can absorb energy from the magnetic field $\vec{H}$ of the wave, and its permanent magnetic dipole $\vec{\mu}_{O_2}$ is reoriented according to a Boltzmann distribution determined by the

factor $\exp[-\vec{\mu}_{O_2}\vec{H}]/kT$. This absorption appears with no particular resonance frequency (except zero) and has the following expression [55]:

$$\kappa_{\nu,\text{Debye}}(m^{-1}) = \frac{8\pi^2 N \mid \mu \mid^2}{3ckt} \frac{\nu^2 \Delta\nu}{\nu^2 + \Delta\nu^2} \tag{29}$$

where $\Delta\nu$ is now the relaxation frequency (see below) above which the dipoles can no longer follow the field. For O_2 in the atmosphere, this absorption has to be taken into account at least below 400 GHz [56]. The Debye spectrum of O_2 is introduced in ATM according to (29) with the relaxation frequency, directly related to the mean lifetime between collisions, equal to $0.053\,69 \cdot PT^{-0.8}$ GHz[2]. For the units used in this paper (see Section III,) (30) will give: $\kappa_{\nu\text{Debye}}(m^{-1}) = 2.32 \cdot 10^{-4} p_d T^{-2} \nu^2 \Delta\nu/(\nu^2 + \Delta\nu^2)$.

C. Pseudocontinua in ATM

In our ATM model, we introduce collisionally induced dry absorption and longwave (foreign) pseudocontinuum water vapor absorption derived from our previous FTS measurements performed on top of Mauna Kea, HI. For both terms, we use ν^2 frequency power laws, with the coefficients as determined by Pardo *et al.* [20]

$$\kappa_{c,H_2O} = 0.0315 \cdot \left(\frac{\nu}{225}\right)^2 \left[\frac{p_w}{1013} \cdot \frac{p_d}{1013}\right] \cdot \left(\frac{300}{T}\right)^3 \tag{30}$$

$$\kappa_{c,\text{dry}} = 2.612 \cdot 10^{-6} \left(\frac{p_d}{1013}\right)^2 \left(\frac{300}{T}\right)^{3.5} \left(\frac{\nu}{225}\right)^2. \tag{31}$$

We are continuing to collect data under various atmospheric (humidity) conditions, and so the coefficients will no doubt be refined somewhat in the future. The validity of these expressions is restricted to frequencies ≤ 1.1 THz (the upper limit of our current data). Above 1.1 THz, it is better to use the $N_2 - N_2$ continuum formulation of Borysow and Frommhold [57] (far-infrared collision-induced spectrum of nitrogen) scaled upward by a factor of 1.29. The 29% correction has been found necessary to fit our FTS data [20] and accounts for additional collisional mechanisms such as $N_2 - O_2$ and $O_2 - O_2$ collisions. The simple ν^2 law used above loses validity beyond ~1 THz as the center of the band (at $\nu \simeq 2.4$ THz) is approached. It could be possible in the future to observe this rollover with further higher frequency FTS measurements.

VIII. Experimental Basis

As described above, a series of FTS measurements on Mauna Kea [19], [20] are providing a data set against which we are testing and refining the model. Some results obtained during extremely dry conditions allowed us to separately measure for the first time the submillimeter wet and dry pseudocontinua terms [20]. After revising the model to take those results into account, our new FTS data obtained during 2000 and 2001, are fitted extremely well. As an example, we present here two measurements obtained in March and July 2000 and their corresponding fits (Fig. 1). When completed, the whole data set will be presented in a future paper, along with our final best fit coefficients for the continuum-like opacities.
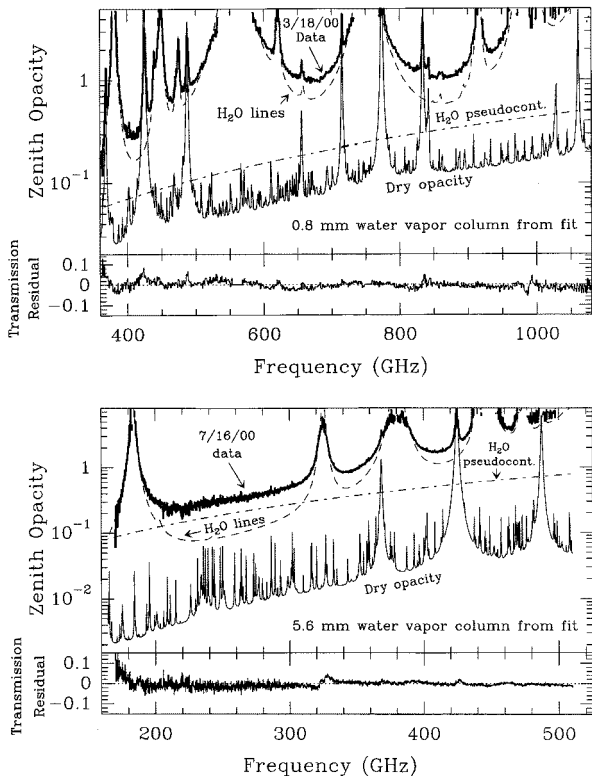
Fig. 1. FTS zenith atmospheric opacity spectra obtained on Mauna Kea in March and July 2000 and best fit opacity contributions. The estimated water vapor columns differ by a factor of seven. Because the curve $\tau_{fit}(\nu)$ matches the data so well, the fit residuals are shown as the transmission difference $(exp[-\tau_{\mathrm{meas}}] - exp[-\tau_{\mathrm{fit}}])$. The fitting routine that produced these results is based on the radiative transfer code described in this paper and uses only the precipitable water vapor column as a free parameter (P/T profile is fixed from the readings of the Mauna Kea weather station, our own handheld thermo/hygrometer, and Hilo airport radiosoundings).

IX. PREDICTIONS FOR SUBMILLIMETER SITES

During the past few years, new ground-based astronomical observatories have been built to allow access to the submillimeter range of the electromagnetic spectrum. Potential sites are now being tested for more ambitious instruments such as the Atacama Large Millimeter Array (ALMA). All of these are remote high-altitude sites. For our simulations, we have selected three sites of interest for submillimeter astronomy: Mauna Kea, HI (LAT $= 19 : 46 : 36$, LONG $= -155 : 28 : 18$; home of the Caltech Submillimeter Observatory, James Clerk Maxwell telescope, and Smithsonian Submillimeter Array); Chajnantor, Chile (LAT $= -23 : 06$, LONG $= -67 : 27$, the site selected for ALMA); and the Geographic South Pole (site of the Antarctic Submillimeter Telescope and Remote Observatory).

To analyze the differences between these sites, we have run our current best fit ATM model for typical T/P profiles obtained from *in situ* radiosonde measurements and compared predictions for the same zenith precipitable water vapor columns (N_{H_2O}, in mm). We have used 0.15, 0.5, and 1.0 mm of water to reproduce conditions ranging from outstanding to good zenith submillimeter transmission. Of course, the percentage of time for which the integrated column of water vapor is below a given value is different for each site, and that contributes to make one site superior to another. Here we focus on the differences for a
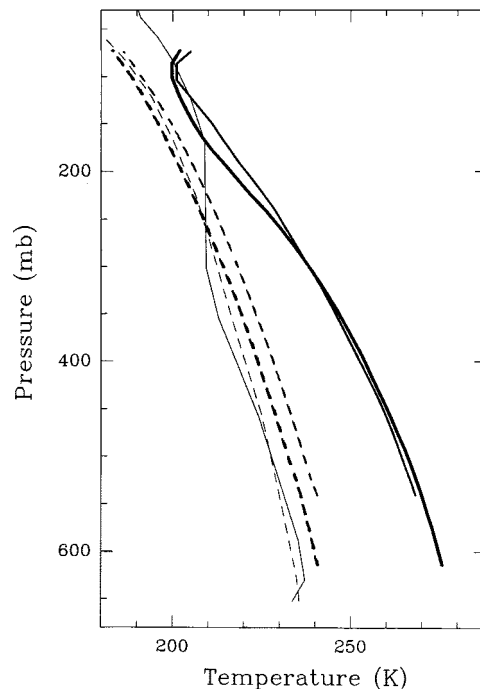

Fig. 2. Atmospheric T/P profiles (solid lines) for the three sites considered in our calculations (see text). To make a comparison of the different sites under the same columns of water vapor, we have introduced moisture profiles with a total of 0.15, 0.5, and 1.0 mm for each site. In the figure, we show the dewpoint temperatures (dashed lines) that correspond to 0.5 mm of water vapor column above each site. Note that the moisture would be above saturation for the South Pole winter profile in that case (below saturation for 0.15 mm).

given, common amount of water vapor. The T/P profiles used in the simulations have been obtained from the following.

1) Mauna Kea site (MK): Radiosoundings launched twice daily from the nearby Hilo airport ($\sim$25 mi away), truncated on the lower end at 4.1 km. The T/P profile considered here is the average for the period November 1, 1999 to January 31, 2000 (winter).

2) Chajnantor (CH): The Chajnantor radiosonde campaign is a collaboration between the National Radio Astronomy Observatory, the European Southern Observatory, Cornell University, the Smithsonian Astrophysical Observatory, and the Japanese LMSA project. The T/P profile considered here is the average (from 28 radiosoundings) corresponding to the November 1999 campaign (summer).

3) Geographic South Pole (SP): The radiosonde T/P profiles used here come from *in situ* winter-time measurements provided by Chamberlin [58].

The three profiles we have used are plotted on Fig. 2. Although the MK and CH profiles correspond to different seasons, they are fairly similar except for the starting altitude/pressure. We know that on Mauna Kea, the nighttime ground-level temperatures typically fall within the range 273$\pm$5 K year round, and the same seems to apply to Chajnantor. The SP site is much colder and also lower.

We first compare the transmission for the three sites under the same water vapor column. We begin with the 0.15-mm case, an outstanding situation for ground-based submillimeter-wave
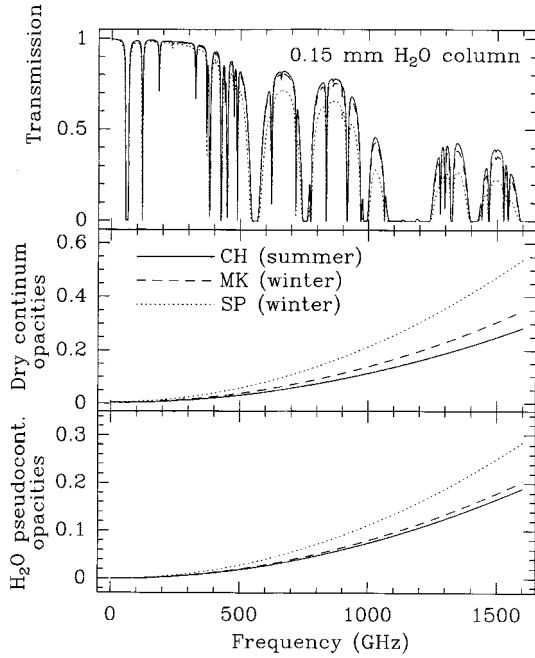
Fig. 3. Calculated atmospheric transmissions and continuum-like opacities for the three atmospheric profiles of Fig. 2. Solid, dashed, and dotted line indications apply also for the upper panel. Minor gases have been removed for clarity.
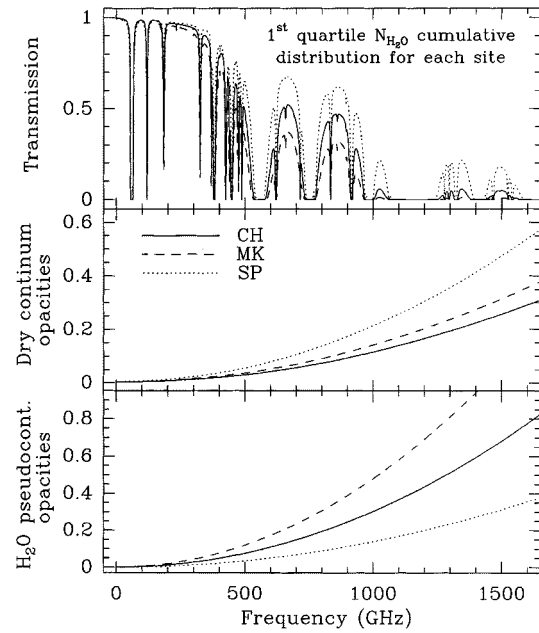

Fig. 4. Calculated atmospheric transmissions and continuum-like opacities for the three atmospheric T/P profiles of Fig. 2 but considering now N_{H_2O} amount at the 25% quartile of the cumulative N_{H_2O} function for wintertime in the three sites. Minor gases have been removed for clarity. Solid, dashed, and dotted line indications as in Fig. 3. As indicated in the text, the distributions used here were derived from different methods.

astronomy. Such a low water vapor column seems to be a lower limit for all three sites considered here. FTS data have already shown water vapor columns very close to that value [20], [59], [60]. At the South Pole, the cold winter temperatures and the saturation of water vapor indicate that such conditions would happen quite often at this site (note that $N_{H_2O} = 0.5$mm gives an oversaturation for SP winter over an important vertical range). The comparison of the calculated atmospheric transmissions for this case is shown in Fig. 3.

It may seem surprising from this figure that the worst transmission is predicted for the South Pole site. This result arises from the combination of several factors.

1) The higher ground-level pressure and the lower temperature both make the line absorption broader (22).
2) The dry continuum (middle panel of Fig. 3) and H_2O pseudocontinuum (bottom panel of Fig. 3) terms are both higher due to the higher pressures as well [(30) and (31)].
3) The partition function is a positive temperature power law [see, e.g., (15)], causing absorption in low energy levels to increase as temperature decreases.

Under equal and extremely low water vapor column conditions, the transmission in the high-frequency atmospheric windows (above 980 GHz) is then nearly a factor of two lower at SP than at CH, while MK is only about 10% worse than CH. In other words, the transmissions above 980 GHz in extremely dry conditions at the CH and SP sites would be similar if CH had twice the water vapor column of the SP site. This does not automatically mean that Chajnantor is a superior site to the South Pole, because the frequency distribution of N_{H_2O} also needs to be taken into account. This suggests that to evaluate sites, T/P data need to be weighted by N_{H_2O} statistics, or better yet, direct

transmission measurements should be compared. Here we have taken N_{H_2O} cumulative distributions from [61] and have performed a direct comparison of the three 25% quartiles for each site in winter (Fig. 4). The South Pole distributions are derived from radiosonde flights. A full description can be found in [62]. In this comparison, SP is best.

A. Atmospheric Dispersive Phase

Another issue of importance, primarily for interferometry, is the atmospheric phase delay. Present-day radio interferometers are mostly limited to frequencies below 350 GHz. Dispersive phase delay increases in importance as the frequency increases into the submillimeter domain because of the strength of the atmospheric lines involved in both absorption and dispersion. Using the complex line shape of (27), we have calculated the derivative of the dispersive phase delay with respect to the water vapor column $\partial\phi/\partial N_{H_2O}$ (this derivative will be called the *differential phase* and is provided in deg/μm here). The differential phase as a function of frequency has been plotted for the Chajnantor site in Fig. 5 (where the curve is restricted to those frequencies where the transmission is above 10% when the precipitable water vapor column is 0.3 mm, i.e., very good conditions for single-dish submillimeter observations). Another useful quantity plotted in the same figure is the derivative of the dispersive phase delay with respect to the sky brightness temperature ($T_{B,sky}$), since this function relates the dispersive phase correction between two antennas to a measurable physical parameter ($T_{B,sky}$). Note, however, that whereas the differential phase described above depends only on ΔN_{H_2O}, this new quantity depends on the absolute H_2O column as well. The curve
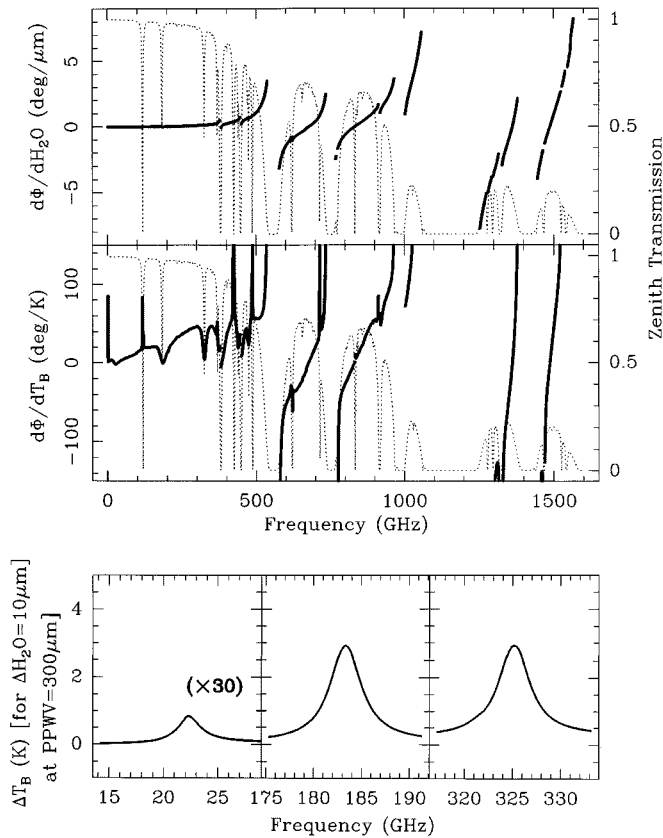
Fig. 5. Upper panel: Derivative of the dispersive phase delay respect to the water vapor column (*differential phase* in text; this derivative is independent of the water vapor column) as a function of frequency, superposed on the Chajnantor atmospheric transmission curve for 0.3 mm of water vapor. Middle panel: Derivative of the dispersive phase delay with respect to the sky brightness temperature for 0.3 mm H_2O column. Lower panel: $\left[\partial T_b(\nu)/\partial N_{H_2O}\right]_{N_{H_2O}=0.3\mathrm{mm}}$ around the water vapor resonances at 22.23, 183.31, and 325.15 GHz.

plotted here corresponds to $\partial\phi/\partial T_b(\nu)$ at $N_{H_2O} = 0.3$mm. On the same figure, we plot the curves $\partial T_b(\nu)/\partial N_{H_2O}$ around the water vapor lines at 22.23, 183.31, and 325.15 GHz also for $N_{H_2O} = 0.3$mm. Of these, the lines at 183.31 and 325.15 GHz are the best choices to monitor water vapor path differences between antennas for differential phase corrections in the range of water vapor columns that allow submillimeter observations to be carried out. The reason for this is that the center of these lines displays a brightness temperature range of $\sim$170 K for water vapor columns between 0.15 and 1.5 mm (for larger H_2O columns, transmission at the center of the 650 and 850 GHz atmospheric windows falls below 15%), a range that is unmatched by any other water vapor line below 1 THz.

As seen in Fig. 5, the differential phase becomes much more important in the submillimeter domain than it is at millimeter wavelengths, so its correct estimation and the selection of the best means of monitoring water vapor column differences between different antennas are essential for ground-based submillimeter interferometry. For example, the differential phase is 0.0339 deg/μm at 230 GHz, whereas it is -0.4665 and 0.2597 deg/μm at 650 and 850 GHz, respectively, roughly an order of magnitude larger.
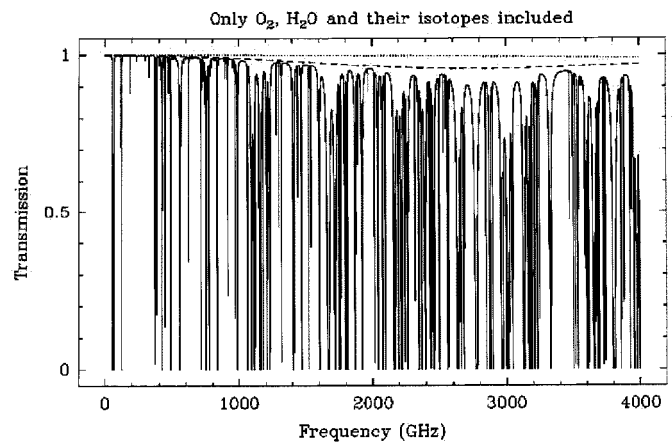

Fig. 6. Atmospheric transmission expected for SOFIA in the range 1–4000 GHz. The trace gases and O_3 have been removed for clarity (for an idea of their effect see next figure). The H_2O pseudocontinuum (dotted line) is expected to be negligible, but the dry continuum (dashed line) will contribute up to an opacity of 0.04.
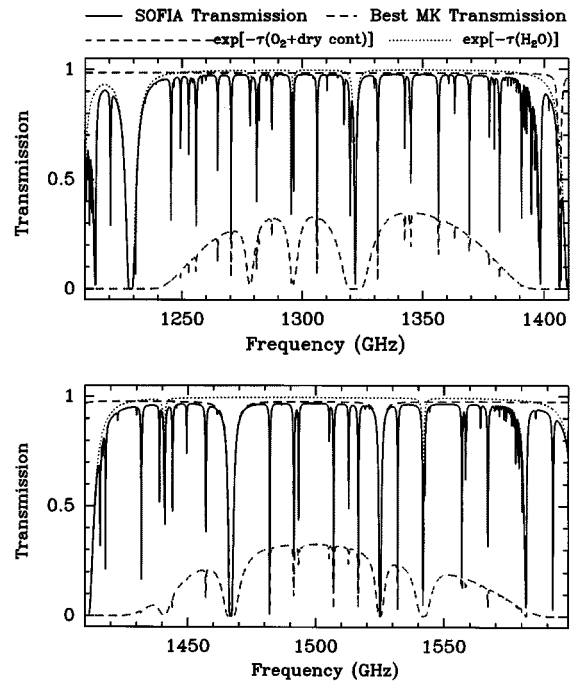

Fig. 7. Zoom of the SOFIA transmission around 1300 and 1500 GHz compared to the transmission expected from the ground in the best ever recorded conditions ($\sim$ 185 μm) of water vapor. The local importance of O_3 and trace gases is stressed in these panels.

B. Atmospheric Spectrum for SOFIA

Finally, we have performed one further simulation of the zenith atmospheric transmission. This one is for the 1–4000 GHz range above 13.2 km, the operating altitude of the future Stratospheric Observatory for Infrared Astronomy (SOFIA) [63] shown in Figs. 6 and 7. The SOFIA sky spectrum is mainly dominated by ozone, H_2O, and O_2 resonances, but there is also a small dry continuum, modeled here according to [57] with the 29% correction given in Section VII-C, which is responsible for about 4% absorption at 3 THz. On the other hand, the H_2O pseudocontinuum at this altitude is negligible.

X. Conclusion

Our current atmospheric radiative transfer model, ATM, has been described in detail. It includes the absorption and phase-delay effects due to all H_2O, O_2, and O_3 resonances up to 10 THz. It also includes semiempirical continuum-like terms derived from our FTS measurements on Mauna Kea. The model is applicable to fields as diverse as astronomy, remote sensing, and communications.

Based upon our current best fit model, it is possible to show that Chajnantor (the future site of ALMA) provides significantly better transmission than the South Pole for equal water vapor columns. In fact, below 0.5 mm of H_2O, equivalent transmissions occur at the two sites above 980 GHz with a factor of two higher water vapor present at Chajnantor. This is important to fold into comparisons of the two sites.

The first simulations of dispersive phase delay have been presented here as a first step for selecting strategies for its correction in future submillimeter interferometers such as ALMA.

Other simulations have been devoted to the atmospheric transmission for the operating altitude of the SOFIA instrument, showing the many details of the atmospheric transmission spectrum as it appears there. In particular, O_3 and trace gas opacities become locally important and need to be well modeled.

References

[1] H. J. Liebe, "MPM — An atmospheric millimeter-wave propagation model," *Int. J. Infrared Millimeter Waves*, vol. 10, pp. 631–650, 1989.

[2] H. J. Liebe, G. A. Hufford, and M. G. Cotton, "Propagation modeling of moist air and suspended water/ice particles at frequencies below 1000 GHz," in *Proc. AGARD 52nd Specialists' Meeting Electromag. Wave Propagation Panel*, Palma de Mallorca, Spain, 1993.

[3] E. Grossman, *AT User's Manual*. Boulder, CO: Airhead Software, 1989.

[4] J. Cernicharo, "ATM: A program to compute atmospheric transmission between 0–1000 GHz,", Internal Rep. Institut de Radiostronomie Millimétrique (IRAM), 1985.

[5] ——, Ph.D dissertation, Université de Paris VII, 1988.

[6] J. R. Pardo, "Etudes de l'atmosph \ere terrestre au moyen d'observations dans les longueurs d'onde millimetriques\ etriques et submillimetriques\ ∕etriques," Ph.D dissertation, Université de Paris VI, 1996.

[7] L. S. Rothman, R. R. Gamache, R. H. Tipping, C. P. Rinsland, M. A. H. Smith, D. B. Chris, V. D. Malathy, J.-M Flaud, C. Camy-Peyret, A. Perrin, A. Goldman, S. T. Massie, L. R. Brown, and R. A. Toth, "HI-TRAN database: 1991 and 1992 editions," *J. Quantum Spectrosc. Radiat. Transfer*, vol. 48, pp. 469–507, 1992.

[8] H. M. Pickett, R. L. Poynter, E. A. Cohen, M. L. Delitsky, J. C. Pearson, and H. S. P. Muller, "Submillimeter, millimeter, and microwave spectral line catalog," *J. Quantum Spectrosc. Radiat. Transfer*, vol. 60, pp. 883–890, 1998.

[9] N. Jacquinet-Husson, E. Arié, J. Ballard, A. Barbe, G. Bjoraker, B. Bonnet, L. R. Brown, C. Camy-Peyret, J. P. Champion, A. Chédin, A. Chursin, C. Clerbaux, G. Duxbury, J. M. Flaud, N. Fourrié, A. Fayt, G. Graner, R. Gamache, A. Goldman, G. Vl, G. Guelachvili, J. M. Hartmann, J. C. Hilico, J. Hillman, G. Lefèvre, E. Lellouch, S. N. Mikhaïlenko, O. V. Naumenko, V. Nemtchinov, D. A. Newnham, A. Nikitin, J. Orphal, A. Perrin, D. C. Reuter, C. P. Rinsland, L. Rosenmann, L. S. Rothman, N. A. Scott, J. Selby, L. N. Sinitsa, J. M. Sirota, A. M. Smith, K. M. Smith, G. T. Vl, R. H. Tipping, S. Urban, P. Varanasi, and M. Weber, "The 1997 GEISA spectroscopic databank," *J. Quantum Spectrosc. Radiat. Transfer*, vol. 62/2, pp. 205–254, 1999.

[10] J. R. Pardo, M. Gérin, L. Pagani, and C. Prigent, "Evidence of the Zeeman splitting in the $2(1)- > 0(1)$ rotational transition of the stmospheric $^{16}O^{18}O$ molecule from ground-Based measurements," *J. Quantum Spectrosc. Radiat. Transfer*, vol. 54/6, pp. 931–931, 1995.

[11] J. R. Pardo, M. Gérin, C. Prigent, J. Cernicharo, G. Rochard, and P. Brunel, "Remote sensing of the mesospheric temperature profile from close-to-nadir observations: discussion about the capabilities of the 57.5-62.5 GHz frequency band and the 118.75 GHz single O_2 line," *J. Quantum Spectrosc. Radiat. Transfer*, vol. 60/4, pp. 559–571, 1998.

[12] J. R. Pardo, M. Ridal, D. Murtagh, and J. Cernicharo, "Microwave temperature and pressure measurements with the Odin satellite: I. Observation method," *Can. J. Phys.*, 2002, to be published.

[13] J. R. Pardo, M. Mishchenko, C. Prigent, and W. Rossow, , 2001, to be published.

[14] S. Chandrasekhar, *Radiative Transfer*. Oxford, U.K.: Oxford Univ. Press, 1960.

[15] H. W. Kroto, *Molecular Rotation Spectra*. New York: Wiley, 1975.

[16] J. K. G. Watson, *Aspects of Quartic and Sextic Centrifugal Effects on Rotational Energy Levers*, J. R. Durig, Ed, Amsterdam: Elsevier, 1977, vol. 6.

[17] C. Camy-Peyret and J. M.Flaud, "Line positions and intensities in the $\nu_2 \, band \, of \, H_2O$," *Molecular Phys.*, vol. 32/2, pp. 523–537, 1976.

[18] G. Herzberg, *Spectra of Diatomic Molecules*. New York: Van Nostrand Reinhold, 1950.

[19] E. Serabyn, E. W. Weisstein, D. C. Lis, and J. R. Pardo, "Submillimeter FTS measurements of atmospheric opacity above Mauna Kea," *Appl. Opt.*, vol. 37/12, pp. 2185–2198, 1998.

[20] J. R. Pardo, E. Serabyn, and J. Cernicharo, "Submillimeter atmospheric transmission measurements on Mauna Kea during extremely dry El Niño conditions : Implications for broadband opacity contributions," *J. Quantum Spectrosc. Radiat. Transfer*, vol. 68/4, pp. 419–433, 2001.

[21] P. Chen, J. C. Pearson, H. M. Pickett, S. Matsuura, and G. A. Blake, "Submillimeter-wave measurements and analysis of the ground and $\nu_2 = 1$ states of water," *Astrophys. J. Suppl. Ser.*, vol. 128, pp. 371–385, 2000.

[22] M. Matsushima *et al.*, "Frequency measurement of pure rotational transitions of H_2O from 0.5 to 5 THz," *J. Mol. Struct.*, vol. 352/353, pp. 371–378, 1995.

[23] P. A. Helminger and F. C. de Lucia, "Centrifugal distortion analysis of the ground vibrational states of $H_2^{17}O \, and \, H_2^{18}O$," *J. Mol. Spectrosc.*, vol. 70, pp. 263–269, 1978.

[24] S. P. Belov, I. N. Kozin, O. L. Polyansky, M. M. T. Yu, and N. F. Zobov, "Rotational spectrum of the $H_2^{16}O$ molecule in the (010) excited vibrational state," *J. Mol. Spectrosc.*, vol. 126, pp. 113–117, 1987.

[25] F. C. de Lucia, R. L. Cook, P. Helminger, and W. Gordy, "Millimeter and submillimeter wave rotational spectrum and centrifugal destortion effects of HDO," *J. Chem. Phys.*, vol. 55, pp. 5334–5334, 1971.

[26] L. R. Zink and M. Mizushima, "Pure rotational far-infrared transtions of $^{16}O_2$ in its electronic and vibrational ground state," *J. Mol. Spectrosc.*, vol. 125, pp. 154–158, 1987.

[27] W. Steinbach and W. Gordy, "Microwave spectrum and molecular constants of $^{16}O^{18}O$," *Phys. Rev.*, vol. A11, pp. 729–731, 1975.

[28] W. Gordy and R. L. Cook, *Microwave Molecular Spectra*. New York: Wiley, 1984.

[29] H. M. Pickett *et al.*, "The vibrational and rotational spectra of ozone for the (0, 1, 0) and (0, 2, 0) states," *J. Mol. Spectrosc.*, vol. 128, pp. 151–171, 1988.

[30] J. M. Flaud *et al.*, "The ν_1 and ν_3 Bands of $^{16}O_3$: Line positions and intensities," *J. Mol. Spectrosc.*, vol. 124, pp. 209–217, 1987.

[31] ——, "The ν_2 Bands of ^{16}O and $^{16}O^{16}O^{18}O$: Line positions and intensities," *J. Mol. Spectrosc.*, vol. 133, pp. 217–223, 1987.

[32] C. P. Rinsland *et al.*, "The ν_2 Bands of $^{16}O^{17}O^{16}$ and ^{16}O and $^{16}O^{16}O^{17}O$: Line Positions and Intensities," *J. Mol. Spectrosc.*, vol. 149, pp. 474–480, 1991.

[33] A. Andreev *et al.*, "Submillimeter wave spectrum and Molecular Constants of N_2O," *J. Mol. Spectrosc.*, vol. 62, pp. 125–148, 1976.

[34] P. A. Helminger and F. C. de Lucia, "The submillimeter wave spectrum of $^{32}S^{16}O_2 ^{32}S^{16}O_2(\nu_2)$, and $^{34}S^{16}O_2$," *J. Mol. Spectrosc.*, vol. 111, pp. 66–72, 1985.

[35] W. C. Lane *et al.*, "Analysis of nu_2 of H $_2^{33}$ and H $_2^{34}$ S," *J. Mol. Spectrosc.*, vol. 111, pp. 320–326, 1985.

[36] N. Semmoud-Monnanteuil *et al.*, "New measurements in the Millimeter-wave Spectrum of $^{14}N \, ^{16}O_2$," *J. Mol. Spectrosc.*, vol. 134, pp. 176–182, 1989.

[37] U. Fano, "Pressure broadening as a prototype of relaxation," *Phys. Rev.*, vol. 131, pp. 259–268, 1963.

[38] J. H. Van Vleck and V. F. Weisskopf, "On the shape of collision-broadened lines," *Rev. Mod. Phys.*, vol. 17, pp. 227–236, 1945.

[39] S. A. Zhevakin and A. P. Naumov, "Refraction of millimetre and sub-millimetre radio waves in the lower atmosphere," *Izv. Vysshik Chebn. Zavedenii Radiofiz*, vol. 6, pp. 674–694, 1963.

[40] B. Labani, J. Bonamy, D. Robert, J. M. Hartmann, and J. Taine, "Collisional broadening of rotation-vibration lines for asymmetric top molecules. I. Theoretical model for both distant and close collisions," *J. Chem. Phys.*, vol. 84, pp. 4256–4267, 1986.

[41] A. Barbe, L. Regalia, J. Plateaux, P. H. Von der, and X. Thomas, "Temperature dependence of N_2 and O_2 broadening coefficients of ozone," *J. Mol. Spectrosc.*, vol. 180, pp. 175–182, 1996.

[42] B. J. Connor *et al.*, "Pressure broadening of millimeter-wave lines ozone lines by atmospheric gases," *J. Mol. Spectrosc.*, vol. 117, pp. 15–29, 1986.

[43] R. R. Gamache *et al.*, "Temperature dependence of N_2-broadened halfwidths of water vapor: The pure rotation and ν_2 bands," *J. Mol. Spectrosc.*, vol. 128, pp. 360–369, 1985.

[44] S. Bouazza *et al.*, "Measurements and calculations of room-temperature ozone line-broadening by N_2 and O_2 in the $\nu_1 + \nu_3$ band," *J. Mol. Spectrosc.*, vol. 157, pp. 271–271, 1993.

[45] E. F. Fishbein *et al.*, "Validation of UARS microwave limb sounder temperature and pressure measurements," *J. Geophys. Res.*, vol. 101/D6, pp. 9983–10 016, 1996.

[46] H. A. Kramers, "some remarks on the theory of absorption of x rays," *Nature*, vol. 117, pp. 775–775, 1926.

[47] R. L. de Krönig, "On the theory of dispersion of X rays," *J. Opt. Soc. Amer.*, vol. 12, pp. 547–547, 1926.

[48] P. W. Rosenkranz, "Interference coefficients for overlapping oxygen lines in air," *J. Quantum Spect. Radiat. Transfer*, vol. 39/4, pp. 287–297, 1988.

[49] E. P. Gross, "Collision broadening," *Phys. Rev.*, vol. 97, pp. 395–403, 1955.

[50] "Interaction model of microwave energy and atmospheric variables ,", Environmental Res. Technol., Inc. final report contract no. NAS8-26275, Feb. 1971.

[51] D. P. Rice and P. A. R. Ade, "Absolute measurements of the atmospheric transparency at short millimetre wavelengths," *Infra. Phys.*, vol. 19, pp. 575–584, 1979.

[52] S. A. Clough, F. X. Kneizys, and R. W. Davies, "Line shape and the water vapor continuum," *Atmos. Res.*, vol. 23, pp. 229–241, 1989.

[53] J. W. Waters, "Absorption and emission by atmospheric gases," in *Methods Experimental Physics*. Orlando, FL: Academic, 1976, vol. 12B, ch. 2.3.

[54] Q. Ma and R. H. Tipping, "Water vapor continnum in the millimeter spectral region," *J. Chem. Phys.*, vol. 93, pp. 6127–6139, 1990.

[55] P. Debye, *Polar Molecules*. Lancaster, U.K.: Lancaster Press, 1929.

[56] P. W. Rosenkranz, "Absorption of microwaves by atmospheric gases," in *Atmospheric Remote Sensing by Microwave Radiometry*, M. Janssen, Ed. New York: Wiley, 1993, ch. 2.

[57] A. Borysow and L. Frommhold, "Collision-induced rototranslational absorption spectra of N_2 -N_2 pairs for temperatures from 50 to 300 K," *Astrophys. J.*, vol. 311, pp. 1043–1057, 1986.

[58] R. A. Chamberlin and J. Bally, "The observed relationship between the south pole 225-GHz atmospheric opacity and the water vapor column density," *Appl. Opt.*, vol. 33/6, pp. 1095–1095, 1994.

[59] S. Matsushita, H. Matsuo, J. R. Pardo, and S. Radford, "FTS measurements of submm-wave atmospheric opacity at Pampa la Bola II: Supra-THz windows and model fitting," *Pub. Astron. Soc. Jpn.*, vol. 51/5, pp. 603–610, 1999.

[60] S. Paine, R. Blundell, D. C. Papa, J. W. Barrett, and S. J. E. Radford, "A Fourier transform spectrometer for measurement of atmospheric transmission at submilimeter wavelengths," in *PASP*, vol. 112/767, 2000, pp. 108–118.

[61] A. P. Lane, "Submilimeter Transmission at South Pole," in *Astrophysics from Antarctica*, G. Novak and R. H. Landsberg, Eds: ASP Conference Series, 1998, vol. 141, pp. 289–295.

[62] R. A. Chamberlin, "South Pole submilimeter sky opacity and correlations with radiosonde observations ," *J. Geophys. Res.*, vol. 106, no. D17, pp. 20–101, 2001.

[63] E. E. Becklin, "The far infrared and submilimeter universe," in *Proc. ESA Symp. Stratospheric Observatory for Infrared Astronomy (SOFIA)*, Grenoble, France, Apr. 15–17 , 1997, ESA SP-401, pp. 201–206.

Juan R. Pardo received the degree in physics from Complutense University of Madrid, Spain, in 1991 and the Ph.D. degree in astrophysics and spatial techniques from Pierre et Marie Curie University, Paris, France, in 1996.

Since then, he has been a Postdoctoral Research Fellow supported by the U.S. National Science Foundation at the NASA-Goddard Institute for Space Studies, New York, and at the California Institute of Technology, Pasadena. In 2001, he joined the Consejo Superior de Investigaciones Científicas, Madrid, as a Research Associate. His main research interests are microwave and IR spectroscopy, observational techniques in submillimeter astronomy, interstellar and circumstellar media, radiative transfer in planetary atmospheres, and terrestrial and planetary remote sensing from ground and satellite plattforms. He has made several contributions to these areas in the past, including the ATM model presented in this paper.

José Cernicharo received the Docteur d'Etatès Sciences (Ph.D.) degree in physics from Paris VII University, Paris, France, in 1988.

He was a Research Scientist with the Centre National de La Recherche Scientifique from 1983 to 1988. In 1988, he joined the Spanish National Observatory (OAN). Since 1996, he has been a Research Professor with the Spanish Consejo Superior de Investigaciones Científicas. In 2000, he was a Visiting Scientist for six months at the California Institute of Technology, Pasadena. His main research interests concern the determination of physical and chemical properties of interstellar and circumstellar media through observations in the millimeter, submillimeter, and far-infrared domains. During 1988–1992, he was Codirector of the Institute de Radioastronomie Millimétrique, Spain. He has been a Member of the commissioning teams of the 30-m IRAM radiotelecope at Granada, Spain, and of the interferometer of the Institute at Plateau de Bure, France. He has been involved in several technical aspects related to those telescopes, such as the pointing and the determination of the radiation pattern, the determination of the corrections for atmospheric attenuation through the development of a specific radiative transfer model (ATM), and the testing of millimeter receivers and backends. He is currently a Mission Scientists of the Herschel Space Observatory (previously called FIRST) of the European Space Agency. He also serves on several national and international committees, panels, and working groups.

Eugene Serabyn received the Ph.D. degree in physics from the University of California, Berkeley, in 1984.

He then spent two years at the Max Planck Institut für Radioastronomie, Bonn, Germany, before moving to the California Institute of Technology, Pasadena, in 1987. He has also been with the NASA Jet Propulsion Laboratory in Pasadena since 1998. He specializes in novel astrophysical techniques and instrumentation, as well as in the study of the center of the Milky Way, the interstellar medium, the planets, and the terrestrial atmosphere.